10-1976

Soft-x-ray appearance potential spectra of La and Ce from 0 to 1400 eV

R. J. Smith
Iowa State University

M. Piacentini
Iowa State University

J. L. Wolf
Iowa State University

David W. Lynch
Iowa State University, dlynch@iastate.edu

Soft-x-ray appearance potential spectra of La and Ce from 0 to 1400 eV

Abstract
The soft-x-ray appearance potential spectra were measured for La and Ce in the 0-1400-eV range. The 3d and 4dspectra exhibited prominent structure, which is discussed along with x-ray absorption and emission data. The excited electron and the core hole interact strongly, and there is evidence for additional interaction with the projectile electron. The two-density-of-states model of Wendin seems promising for explaining the spectra, but it must be extended to allow for the interaction of the projectile electron with the excited atom. The effects of oxidation are described.

Keywords
Ames Laboratory, excited electron, core hole

Comments
This article is from *Physical Review B* 14 (1976): 3419, doi:10.1103/PhysRevB.14.3419. Posted with permission.

PHYSICAL REVIEW B VOLUME 14, NUMBER 8 15 OCTOBER 1976

Soft-x-ray appearance potential spectra of La and Ce from 0 to 1400 eV*

R. J. Smith,† M. Piacentini,‡ J. L. Wolf,§ and D. W. Lynch
Ames Laboratory-ERDA and Department of Physics, Iowa State University, Ames, Iowa 50010
(Received 14 January 1976)

The soft-x-ray appearance potential spectra were measured for La and Ce in the 0–1400-eV range. The 3*d* and 4*d* spectra exhibited prominent structure, which is discussed along with x-ray absorption and emission data. The excited electron and the core hole interact strongly, and there is evidence for additional interaction with the projectile electron. The two-density-of-states model of Wendin seems promising for explaining the spectra, but it must be extended to allow for the interaction of the projectile electron with the excited atom. The effects of oxidation are described.

I. INTRODUCTION

Soft-x-ray appearance potential spectroscopy (SXAPS) has been developed for studying the electronic configuration and composition of solid surfaces. Briefly, one measures the derivative of the total x-ray fluorescence yield induced by electron bombardment of the surface of the sample. The theory most often cited to describe SXAPS line shapes was originally suggested by Dev and Brinkman,[1] and further developed by Houston and Park[2] to relate the measured SXAPS signals to the self-convolution of the one-electron density of states above the Fermi level E_F. This theory worked quite well for the 3*d* transition metals[3] and some of the simple metals.[4,5] As the technique became more popular, and the types of materials studied increased, discrepancies between theory and experiment appeared for rare earths,[6-12] light elements,[13,14] and 4*d* transition metals.[15,16] A recent review[17] gives a thorough development of the one-electron theory for SXAPS and an extensive summary of its successes and failures. The fundamental reason for the breakdown of this theory is the inadequacy of the assumption that the excited core electron and the scattered projectile electron occupy spatially extended states in the conduction band. For the rare earths, the excited core electron may occupy a 4*f* orbital which is quite localized about the excited ion. For such materials, Wendin[18] has suggested a model for SXAPS incorporating two densities of states, one for the scattered projectile electron and one for the excited ion with an electron-hole pair. One or both of these may contain highly localized states.

We initially chose SXAPS as a means of studying evaporated La films with the hope of locating the position of the 4*f* states above E_F using the one-electron theory cited above. This question had not been answered using other spectroscopic methods and is of interest particularly in superconductivity.[19,20] Measurements of the bremsstrahlung isochromat spectrum of La and Ce (Refs. 21, 22) have provided the best available estimate of the position of the 4*f* states relative to the Fermi level. These results did not completely clarify all the complexities of the SXAPS data.

In Sec. II we describe the spectrometer used in this work and show typical La and Ce spectra obtained with this instrument. We found, as have other workers[12,23] that our results were closely related to soft-x-ray absorption (SXA) data. For both La and Ce we find that portions of the individual 3*d* and 4*d* core excitation line shapes are similar to $d\alpha/dE$, where α is the absorption coefficient, while other models, such as the two-density-of-states model,[21] are needed to explain other portions of the spectra. Sec. III presents our data and an interpretation based on the results from SXA and bremsstrahlung isochromat experiments. We point out some similarities between the SXA and SXAPS techniques which we feel are responsible for the rather simple relationship between the measured results of the two techniques. We also discuss the effects of contamination on the spectra of these reactive metals.

II. EXPERIMENTAL CONSIDERATIONS

In a typical SXAPS experiment, x-ray fluorescence of a target material is excited by electron bombardment. A wire mesh at ground potential electrically isolates the electron source and target from the detection apparatus. The x rays from the target pass through the mesh and strike a photocathode. The resulting photoelectrons are collected by a positively biased pin. This current is then measured as the electron beam energy is swept through the region of threshold excitation for a particular core level. Since the total x-ray yield, and thus the photocurrent, is the sum of the intense bremsstrahlung continuum and the weaker characteristic x rays due to radiative decay of the core hole, a derivative of the total yield is often mea-

sured to enhance the abrupt structure in the threshold region. This derivative can be obtained using the potential modulation technique[24] as was done here, or numerically,[25] when the signal-to-noise ratio permits.

The vacuum system[26] was based on two $1\frac{1}{2}$-in. crosses and one tee. It permitted evaporation of samples through baffles to keep the cathode and detector uncontaminated. Base pressures of 8×10^{-11} Torr were achieved. During sample evaporation the pressure could be held below 10^{-8} Torr and within a few minutes later, an experimental run could be made in the low 10^{-10}-Torr range.

The compact x-ray detector is based on the design of Musket and Taatjes[27] while the circuit is similar to that of Houston and Park.[17] No prefiltering or preamplification other than that of the lock-in amplifier itself was used. Since the rare-earth materials studied give very strong signals, noise limitations were not much of a problem with this detection scheme. Using modulation voltages of about 0.3 V peak to peak the sharpest features observed had a full width of about 1 eV, which places an upper limit on our resolution.

The calibration of the incident electron energy relative to the target Fermi level is given[12] by $E = eV + e\phi + 2kT$. Here V is the applied accelerating potential, e is the electron charge, ϕ is the work function of the tungsten emitter (4.52 eV), and $2kT$ is an average kinetic energy of the electrons leaving the filament at temperature T. We have added a total of 5 eV to our recorded data to obtain the results presented below. The modulation amplitude as introduced here does not add to the average energy of the electron but it can have an effect on the data analysis when trying to determine excitation threshold energies. The controversy over determining binding energies by SXAPS is not settled,[3,28] but with the small modulation amplitudes used here it is not a major consideration. The La and Ca films were evaporated from a tungsten basket. The source materials, supplied by the Ames Laboratory, were spectroscopically checked for purity and found to contain less than 1 ppm of most metalic elements, the largest impurity concentrations being Pr (15 ppm) and Gd (10 ppm). The materials were electropolished just prior to insertion into the vacuum. In spite of these precautions, the films still showed evidence of contamination when evaporated and measured at pressures near 10^{-8} Torr (see later). Usually, after a few evaporations below 10^{-8} Torr, the spectra began to change, presumably due to the depletion of the outer contaminated layer of the source material. The early spectra, recorded at pressures below 10^{-9} Torr and before this source purification occurred, resemble the contaminated-film results obtained at higher pressures. After the source purification occurred, the spectra recorded in the mid-10^{-10}-Torr range were reproducible for several hours after each evaporation.

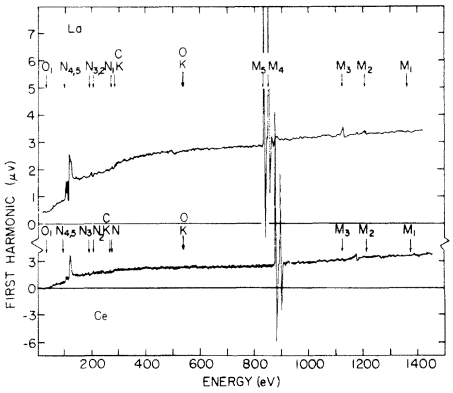

FIG. 1. SXAPS results for La and Ce from 0 to 1400 eV. Recorded with an emission current density, $j=2.8\times10^{-3}$ A/cm^2 at 1200 V, modulation amplitude 0.75 V peak to peak, time constant $\tau=1$ sec. The vertical arrows mark the atomic core binding energies (Ref. 29) for La, Ce, carbon, and oxygen.

Figure 1 shows the first-harmonic spectra of La and Ce from 0 to 1400 eV. The vertical arrows indicate the atomic core binding energies.[29] The low-energy region is characterized by a sloping background due primarily to space-charge-limited beam current. A correction for this nonconstant background can be made and it is sufficient to note that the peak positions are not shifted significantly by this correction.

III. RESULTS AND DISCUSSION

A. La $N_{4,5}$ region

In Fig. 2 we show the $N_{4,5}$ region of the La spectrum. The dashed curve was obtained from our first evaporations. After a few more evaporations from the same source, the upper curve was obtained and the spectra of contaminants diminished so that no oxygen and negligible carbon were detected. The results were confirmed by using a freshly prepared piece of La, presumably less contaminated. The initial evaporation gave results like the dashed curve of Fig. 2, but after only three evaporations, spectra like the solid curve were obtained. We could not identify the composition of the contaminated surfaces and, consequently, whether we refer to the film as "oxide" or "contaminated," we mean simply not a pure metal. Similar spectra for the La $N_{4,5}$ region have been reported previously[9,11] although the peaks A, A' and B, B' were not clearly resolved there. We also

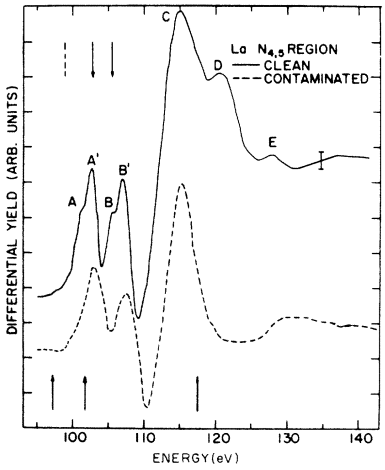

FIG. 2. SXAPS for the La $N_{4,5}$ region. The contaminated-film spectrum is from an earlier evaporation. Conditions were the same as in Fig. 1, except $\tau = 300$ msec here. The clean-film spectrum was obtained within 10 min. after evaporation at a pressure of 5×10^{-10} Torr. The vertical dash marks the atomic $N_{4,5}$ binding energy[29] and the arrows pointing down mark XPS peak positions.[32] The arrows pointing up mark SXA peak positions.[31] The error bar marks the noise level for a single scan. Five scans were averaged. These spectra are on a sloping background, as shown in Fig. 1.

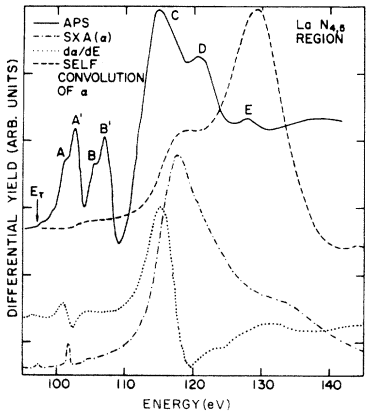

FIG. 3. Comparison of SXAPS model calculations with experiment for the La $N_{4,5}$ region. The solid curve shows our SXAPS while the dash-dot curve shows the SXA data of Rabe.[31] The dotted line is $d\alpha/dE$ and the dashed line is a calculation using the SXA data in our Eq. (2).

resolve a steplike threshold at 97.2 eV.

The derivative of the total x-ray yield, Y_t, resulting from bremsstrahlung and radiative decay of the core hole, in the one-electron approximation, is given by[5,17]

$$\frac{dY_t}{dE} = \frac{dY_B}{dE} + \frac{d}{dE}\left(C\int_0^{E-E_c} N(E-E_c-\epsilon)N(\epsilon)\,d\epsilon\right), \quad (1)$$

where Y_B is the bremsstrahlung yield, E_c is the energy of the core level with respect to E_F, and $N(\epsilon)$ is the density of states above E_F. In obtaining Eq. (1) matrix elements are neglected. Within the limits of these approximations, above the excitation threshold energy E_c, the soft x-ray absorption coefficient $\alpha(E)$, at energy $\hbar\omega = E$, is proportional to the density of empty states $N(E-E_c)$, and substitution into Eq. (1) gives

$$\frac{dY_t}{dE} = \frac{dY_B}{dE} + C\frac{d}{dE}\int_0^{E-E_c} \alpha(E-\epsilon)\alpha(E_c+\epsilon)\,d\epsilon\,. \quad (2)$$

Thus using data from SXA experiments for $\alpha(E)$, an SXAPS spectrum can be calculated and compared with the actual spectrum.[30]

In Fig. 3 we show the clean La spectrum and the absorption coefficient data of Rabe.[31] We also show the derivative of α broadened with a 0.5-eV half-width Gaussian distribution, and the expected line shape using Eq. (2) with $E_c = 102.8$ eV.[32] As previously reported,[33] the latter does not agree with the measured spectrum. The failure of the one-electron model also was observed by other groups for the rare earths.[6,7,9,11] On the other hand, $d\alpha/dE$ peaks in good agreement with our main peak C. At higher energy, the SXAPS of the clean material deviates from $d\alpha/dE$, while the contaminated spectrum shows the dip around 120 eV and the broad band above 130 eV as does $d\alpha/dE$. The low-energy structure in $d\alpha/dE$ is about 5 eV below the corresponding peaks in the SXAPS data.

To a large extent we can explain for La the breakdown of the self-convolution model of Eq. (1) and the partial resemblance to the $d\alpha/dE$ spectrum. For the light rare earths[31,34-38] the SXA data show several small, very sharp lines below the expected $4d$ excitation threshold, and a very broad band, some 10–20 eV wide, above threshold. These results have been interpreted[39-42] as being due to a dipole transition of the type $4d^{10}4f^N \rightarrow 4d^9 4f^{N+1}$. Several arguments support this assignment.[40] The one-electron wave function for the lowest-energy $4f$ orbital of La (Ref. 43) is bound inside the centrifugal potential barrier and greatly overlaps the $4d$ wave function. Since the higher-energy f orbitals are not bound by this barrier, most of the absorption strength from the $4d$ shell will go into transitions to the $4f$ shell. Second, because of the large overlap of the $4d$ and $4f$ wave functions, the exchange interaction between the $4d$ core hole and the $4f^{N+1}$ configuration is strong. This interaction splits the final-state configuration into a multiplet spread over 20 eV. Some of the levels are pushed below the ionization threshold while others are pushed far above it. Most of the d to f oscillator strength goes into the latter terms of the configuration, which then auto-

ionize to the configuration $4d^9 4f^N \epsilon f$, where ϵf is a continuum state. The strength of the broad peak above threshold is observed to decrease as the $4f$ shell is filled. The states below threshold are responsible for the sharp lines observed in SXA, many of which are too closely spaced to be resolved by SXAPS, as will be seen in our Ce results. Calculations based on these arguments have been made using an L-S coupling scheme for the tripositive ions.[36,39,42,44] The agreement with SXA for metallic solids is remarkably good. This is perhaps not unexpected, however, since the relevant transitions are shielded from their environment by the centrifugal potential barrier and the outer shells. Furthermore, studies of the rare-earth compounds reveal very similar SXA spectra,[45] and, in fact, we have measured the SXAPS of LaF_3 and it also resembles the La metal spectrum.[26] An interpretation of SXAPS line shapes in terms of atomiclike transitions, including exchange interaction, rather than in terms of continuous interband transitions, invalidates the assumptions on which the one-electron model is based. Final-state interactions cannot be neglected.

We also can understand to some extent the resemblance of $d\alpha/dE$ to the SXAPS spectrum. For high incident-electron energies, the inelastic scattering probability for electrons in a solid often is described using a dielectric description of the solid.[46] Here, the electron-energy-loss spectrum is related to the complex dielectric function $\tilde{\epsilon} = \epsilon_1 + i\epsilon_2$ of the material via the loss function $\mathrm{Im}[-1/\tilde{\epsilon}(\vec{q}, \Delta E)]$, where $\hbar\vec{q}$ is the momentum transfer and $\Delta E = \hbar\omega$ is the energy loss of the transmitted electron. The energy loss probability is given by[46]

$$P(\Delta E, \theta) \propto \mathrm{Im}[-1/\tilde{\epsilon}(\vec{q}, \Delta E)] = \epsilon_2/(\epsilon_1^2 + \epsilon_2^2) .$$

For small scattering angles θ, we consider the limit of small momentum transfer and replace $\tilde{\epsilon}(\vec{q}, \Delta E)$ by the optical dielectric function $\epsilon(0, \omega) = (n + ik)^2$. Above 50 eV we have $k \ll n \approx 1$, so that $\epsilon_2 \ll \epsilon_1 \approx 1$ and

$$\lim_{q \to 0^+} P(\Delta E, \theta) \propto \frac{1}{(\Delta E)^3} \alpha(\Delta E) .$$

The agreement of electron-energy-loss and SXA data is quite good for the rare earths studied by Trebbia and Colliex.[47] We thus have reason to expect some agreement between SXAPS, which in a sense measures the derivative of $P(\Delta E, \theta)$ and $d\alpha/dE$.[30,48,49] For La, both curves have a strong broad band peaking near 115 eV.

We are still faced, however, with the presence of the extra electron in SXAPS which is not present in the final-state configuration of either SXA or electron-energy-loss measurements. We consider the following picture due to Wendin.[18] Let the initial state of the system consist of the crystal ground state and the state of the projectile electron. We then treat the excitation as a two-step process. We first excite the core electron, forming an excited state of the N-particle system with an electron-hole pair on a certain ion, as in an SXA experiment. We then add the projectile electron to the crystal without interaction with the electron-hole pair, forming an $(N+1)$-particle system. Because the two processes are treated independently, the total probability will be the product of the two single probabilities. For the projectile electron this will be proportional to the conduction-band density of states. We choose to represent it with the bremsstrahlung isochromat spectrum. For the core electron we approximate the transition probability with $\alpha(E)$. The convolution integral of Eq. (1) then becomes

$$\frac{dY}{dE} \propto \frac{d}{dE} \int_0^{E-E_c} N(E - E_c - \epsilon)\alpha(E_c + \epsilon)\, d\epsilon . \qquad (3)$$

We evaluated Eq. (3) for the $N_{4,5}$ region of La, using the bremsstrahlung isochromat spectrum of Liefeld *et al.*[21] and the SXA data of Ref. 31. The spectrum thus obtained is compared with the experimental one in Fig. 4. Structures A, B, and D are reproduced. The reason for the 5-eV shift between the lowest-energy peaks in SXA and SXAPS is now clear. When a particular term of the La^{3+} $4d^9 4f^1$ configuration is excited with fixed energy E_b, the scattered noninteracting projectile electron scans through the $(N+1)$-particle density of states. Since the multiplets in $\alpha(E)$ below the continuum edge are quite sharp, we then measure dN/dE. This gives the peak about 5 eV above threshold in the SXAPS spectrum. We interpret the step at 97.2 eV as the excitation energy E_b for

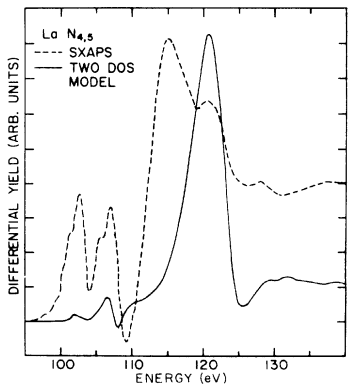

FIG. 4. Comparison of the La $N_{4,5}$ SXAPS (dashed curve) with the two-density-of-states model calculations (solid curve).

the $^3P_1$ state,[41] in agreement with SXA.[31] This is followed by the pair of structures A and A' at 101.4(ΔE = 4.2 eV) and 102.7 eV (ΔE = 5.5 eV). Peak A should correspond to the peak in the bremsstrahlung isochromat spectrum arising from preferential scattering into $4f$ states (see below). The threshold for the $^3D_1$ term should be at 101.3 eV, but is obscured by peaks A, A'. The peaks B, B' occur at 105.5 (ΔE = 4.1 eV) and 106.9 eV (ΔE = 5.6 eV), respectively. The symmetry of A, A' and B, B' seems to rule out the possibility that A corresponds to E_b for the $^3D_1$ term, although a $^3D_1$ threshold in this region, similar to the one at 97.2 eV, may be responsible for the reduced resolution of A and A'.

At higher energies, the optical oscillator strength is almost exclusively in the $^1P_1$ resonance. The excess energy is carried off, not by the scattered projectile electron, but by the excited core electron, as in SXA, in the excitation to the $4d^9 4f$ configuration which then autoionizes to the $4d^9 \epsilon f$ configuration.[50] Peak D could then be a replica of the main peak C resulting from the $^1P_1$ resonance when the projectile electron has sufficient energy to enter a $4f$ state and still excite the $^1P_1$ term. On the other hand, no replica similar to peak D is found in the Ce $N_{4,5}$ spectrum. This will be discussed below. Other explanations have also been offered for the La $N_{4,5}$ structure.[9]

To augment the picture, we must also consider the case when the projectile electron is on the excited ion and interacting with it. The two-density-of-states model is no longer appropriate and we must consider the final-state configuration $4d^9 4f^2$. This configuration is that corresponding to a tripositive Ce ion in the noninteracting scheme. The Ce SXA shows much more structure below threshold than is observed for La, as predicted by atomic calculations,[39,42] and the SXAPS spectrum of Ce shows more structure than that of La. In SXAPS for La the nuclear charge is one less than for Ce so that the number of multiplet terms pulled below threshold could be reduced. We suggest that the splitting A, A' and B, B' may be explained by the interacting scheme, and our Ce results will support this interpretation. The splitting AA' and BB' does not appear to be due to a mixture of pure metal and oxide, since the splitting appears simultaneously with the filling in of the high-energy minimum of Fig. 2. Also, the relative intensity of the two components is always the same, and the peaks for the oxide are shifted to about 0.5-eV higher energy. We rule out the possibility of Ce impurities for our peak D at 120.5 eV. As will be seen later, the main peak in the $N_{4,5}$ SXAPS for Ce occurs at 120 eV. Peak D too might result from the final configuration $4d^9 4f^2$ in La which is a Ce-like state. We would expect the $4d^9 4f^2$ configuration of La to be slightly less bound.

In the contaminated-film spectrum of Fig. 2, the two low-energy peaks are observed without splitting. The threshold has shifted to higher energy, 98.3 eV, and two peaks occur at 102.9 eV (ΔE = 4.7 eV) and 107.6 eV. The main peak C is considerably sharper in this case. Nilsson *et al.*[12] attribute a similar narrowing for the case of Ba to the loss of outer charges to oxygen atoms.

B. La $M_{4,5}$ region

In Fig. 5 we show an expanded plot of the $M_{4,5}$ SXAPS of La. Curve (a) represents the clean material and curve (b) the contaminated surface. The main features of curve (a) in Fig. 5 are the two strong, dispersionlike structures crossing zero at 837.5 and 854 eV, respectively, which we associate with the excitation of the M_5 and M_4 states. These structures correspond to the energy derivative of two peaks, easily detectable in the total yield spectrum. On the low-energy side of each structure there is a pronounced shoulder at 834 and 850 eV and a steplike threshold can be seen at 829.8 eV. The asymmetry in the negative portion of each feature in curve (a) may be due to oxide or other contaminating surface compounds. This is more evident in curve (c), which was obtained from film (a) after being held at 10^{-7} Torr for 30 min. The negative asymmetry has now developed into a shoulder, which corresponds with the negative peak in curve (b). Murthy and Redhead[9] observed a negative peak here, which we believe represents a larger concentration of oxide.[51] The chemical shift between the clean material and the

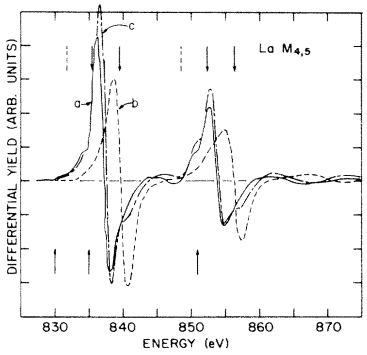

FIG. 5. SXAPS for the La $M_{4,5}$ region: (a) fresh film; (b) from an early evaporation. For these spectra we had $j = 1.0 \times 10^{-3}$ A/cm^2, 0.5 V_{pp} modulation amplitude, $\tau = 1$ sec. The dashed lines are atomic binding energies,[29] the upper arrows are XPS peak positions,[32] and the lower arrows mark SXA peak positions.[52] (c) Film like that of (a) held 30 min at 10^{-7} Torr before measurement. Noise is about the width of the line.

oxide is 2.5 eV, in agreement with x-ray photoemission data.[32]

Figure 6 shows the $M_{4,5}$ SXAPS spectrum of La, compared with the derivative of the absorption-coefficient spectrum[52] and with the SXAPS calculated using Eq. (2), with the threshold energy E_c set at the onset of structure in α. Other values of E_c did not improve the agreement.

We have already discussed the role of exchange in the $4d$-$4f$ transitions for the rare earths. Sugar[53] has performed an analogous calculation for the $3d$ core excitations. Since the exchange interaction is weaker here, the spin-orbit splitting dominates the spectrum. The results of the calculation agree quite well with the observed photoabsorption[52] so we rely again on this final-state interaction picture. The absorption data[52] show a weak peak at 830 eV, followed by a strong peak at 834.9 eV in the M_5 region. The M_4 region has one strong peak at 850.9 eV. The x-ray emission data[54,55] show two strong lines at the same energies as the main absorption peaks. This implies again an atomiclike picture. The excited state has such a long lifetime that the excited electron decays directly into the core hole.

As noted previously, the SXAPS spectrum has the same behavior as SXA: two main features, corresponding to the excitation of the $^3D_1$ and $^1P_1$ states, and the small step at 829.8 eV, which we assign to the excitation threshold of the $^3P_1$ state.

In Sec. III A on the $N_{4,5}$ SXAPS of La we discussed several models that are necessary to interpret the

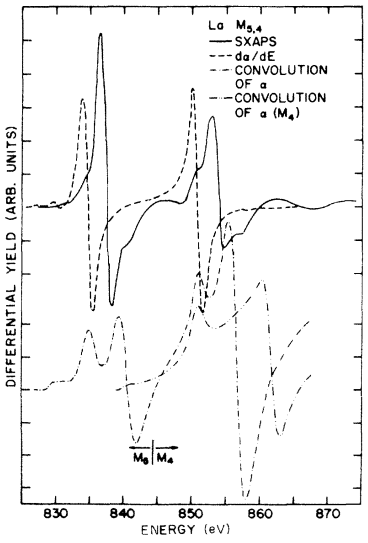

FIG. 6. Comparison of SXAPS model calculations with experiment (solid curve) for the La $M_{4,5}$ region. The dashed curve shows $d\alpha/dE$ using the data of Ref. 52 while the lower curve shows the self-convolution of α using Eq. (2).

data. Some features could be related to $d\alpha/dE$, others to the two-density-of-states model, and others to the interaction model. In the $M_{4,5}$ region it seems that none of these is appropriate. Consider only the M_5 threshold, the M_4 being similar to it. The spectrum of $d\alpha/dE$ is 2.7 eV lower than the main structure (Fig. 6). The two-density-of-states calculation gives the proper line shape, but shifted by about 2.5 eV to higher energies. Finally, the self-convolution model, Eq. (2), gives too much structure (Fig. 6).

Our spectrum is very similar to the M_5 spectrum of Ba,[6] which is formed by a weak step followed by a dispersionlike structure some 6 eV to higher energy. The step was interpreted as the excitation threshold for the $3d \rightarrow 4f$ transitions, and the next structure as arising from a resonant scattering of the incident electron to form a negative-ion bound state with one $3d$ core hole and two $4f$ electrons. Applying the same picture to La, the shoulder at 834 eV thus corresponds to the excitation energy of the $^3D_1$ state and its energy is in good agreement with the absorption and emission line energies of 834.9 eV. The $4f$ states are more bound in La than in Ba. The resonant effect is expected to occur at lower energies, as we observe. Wendin[18] also suggested that the SXAPS structure of Ba may be more a result of a resonance in the continuum background radiation than of an increase in the characteristic soft x rays. Strong support for this suggestion exists for La, where bremsstrahlung isochromat spectra have been measured by Liefeld *et al.*[21] as the projectile electron energy sweeps across the M_5 excitation energy E_m. When the electron energy E_0 is far above or below E_m, the isochromat spectrum shows a peak A at about 6 eV below E_0, interpreted as due to a preferential scattering of the projectile electron into $4f$ states. As soon as $E_0 \sim E_m$, a second peak at the fixed energy E_m starts to develop, indicating that the M_5 state is being excited. Its intensity increases as E_0 increases, reaching a maximum for $E_A \sim E_m$, and then decreases very slowly. This is in agreement with the predictions of the two-density-of-states model. But a second effect takes place simultaneously, which seems to dominate the SXAPS. The peak A in the bremsstrahlung increases enormously when $E_0 > E_m$, up to a maximum at $E_0 \sim 3$ eV in excess of E_m, then decreases again.[56] Strong resonances in the elastic scattering cross section of electrons are well known for atoms just below the excitation energy for certain levels.[57] It seems that we have a somewhat similar phenomenon. The integrated area of the isochromat spectrum measured by Liefeld *et al.*[21] must be proportional to the total yield for La as a function of the incident electron energy. This cal-

culation, performed by Harte *et al.*,[8] is in good agreement with the SXAPS line shape of Fig. 5.

In the contaminated material, the number of La ions near the surface is much smaller and the ions are more separated than in the pure metal. We observe the oxide spectrum to be simpler than that of the metal, implying a reduced contribution from the resonant enhancement of the bremsstrahlung, according to the above model. This suggests that the near-neighbor La atoms may be involved in the enhancement process. It would be very interesting to carry out bremsstrahlung isochromat measurements on La_2O_3 or LaF_3 to investigate this further.

C. Ce $N_{4,5}$ region

Figure 7 shows the $N_{4,5}$ region of the Ce SXAPS, which is quite complex compared to La, and our resolution is insufficient to separate all the expected structures. The main features do resemble La, however, in that we have a region of weak fine structure followed by a large broad band above the expected $N_{4,5}$ threshold. The low-energy region consists of a threshold at 100.7 eV, a shoulder at 103.2 eV, three strong peaks at 105.0, 107.2, and 110.0 eV and a weaker peak at 112.6 eV. Additional weak features at 106.3, 108.2, and 113.7 eV were also observed, but not with good reproducibility. This low-energy region is followed by a large broad peak at 120.1 eV. We do not observe a peak analogous to peak D in La (Fig. 2) but, as shown in Fig. 7, we do observe the filling of a minimum upon successive evaporations. In this figure the film labeled as "contaminated" resulted from the initial Ce evaporation. After a few more evaporations the solid curve was obtained. At the end of our studies the vacuum chamber was filled with oxygen to a pressure of 10^{-3} Torr for 1 h, then pumped out again. The lower broken curve resulted. We note that the depression near 128 eV has returned. There are no major changes in these three curves in the fine-structure region, except possibly a chemical shift of the threshold to about 0.5-eV higher energy for the lowest curve (oxide) and a shift of 1 eV for the middle curve (contaminated). The number of peaks remains constant although their relative intensities have changed somewhat. In Fig. 8 we compare the SXAPS results to the abosrption coefficient α, using the data of Rabe.[31] Also shown are the derivative of α and the derivative of the self-convolution of α as prescribed by the one-electron theory. This last curve shows a peak in agreement with our main peak at 120.1 eV but also predicts a larger peak at higher energy. This is due to the existence of a large peak in α above the chosen threshold, which produces the double-peak structure. The feature at 110 eV in the convolution curve would vanish if the threshold were chosen to be a few eV larger.

The SXA results for Ce have been explained[40,42] quite satisfactorily as for La in terms of exchange-induced multiplet splitting and we proceed to see how well the SXA data describe the SXAPS results. The $d\alpha/dE$ curve predicts a threshold at about 100 eV, followed by peaks at 101, 103.1, 105.5, 107.8, 109.8, and 11.2 eV. The main peak is predicted at 118.5 eV, somewhat below our main peak. Due to the large number of lines observed below threshold in SXA, it is difficult to be conclusive about the correspondence between SXA and SXAPS. By correlating the peaks in $d\alpha/dE$ with the peaks

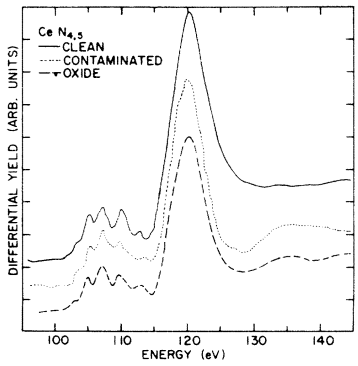

FIG. 7. SXAPS for the $N_{4,5}$ region of Ce. The contaminated-film spectrum is from an early evaporation and the clean-film spectrum is from a later evaporation. The clean film was exposed to oxygen to get the oxide spectrum. The noise level is comparable to that of Fig. 2.

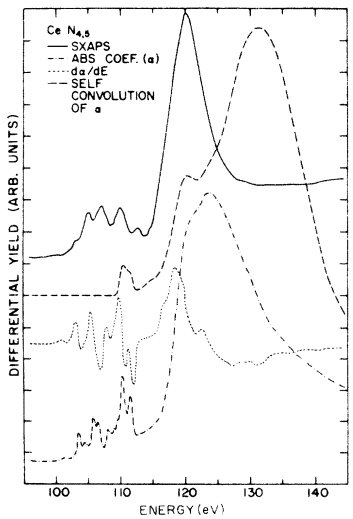

FIG. 8. Comparison of SXAPS model calculations with experiment (solid curve) for the $N_{4,5}$ region of Ce.

in α, and then comparing to the SXAPS results, a tentative assignment can be made. This has been done in Table I. The conclusion reached is that the peaks in SXAPS lie about 2.1 eV above their corresponding optical partners in $d\alpha/dE$. This correspondence has been made on the assumption that SXAPS peaks should lie above the optical peaks, as for La, since the SXA data indicate that such an analysis might apply to all rare-earth metals. Since several of the weaker shoulders in the SXAPS spectrum also fit into this scheme, we feel that improved energy resolution in SXAPS will reveal additional structure. To eliminate possible doubts regarding the assignments in Table I, we have averaged the ΔE values both with and without the weak structures, indicated by an S. The difference in both cases is only 0.1 eV in average separation. Part of the individual deviations from the average values reflects the sharpness of the peaks in SXA and the broadening used for $d\alpha/dE$. For example, with 1-eV broadening the three peaks corresponding to G, K, and L for $d\alpha/dE$ begin to merge into one peak at 109.5 eV.

We are left with the principal failure of the $d\alpha/dE$ curve in predicting the main SXAPS peak at 120.1 eV. We have noted that no bump analogous to peak D in the La spectrum occurred for Ce. The good agreement for La between the main peak in $d\alpha/dE$ and the main SXAPS peak leads one to suspect that the main Ce SXAPS peak results from two peaks which are not resolved, one near 118.5 eV and a second at about 2-eV higher energy. However, we expect to be able to resolve such a pair. Even the second-harmonic spectrum reveals only a slight change of slope in the region of the main peak. An alternative explanation is provided by the interacting electron picture discussed earlier for La. We assume that peak D in La corresponds to the case where both the excited core electron and incident electron occupy $4f$ orbitals *on the same excited ion*. This configuration is $4d^9 4f^2$. The corresponding configuration in Ce is $4d^9 4f^3$. It may be that this configuration with an unpaired $4f$ electron is not bound by the Ce ion potential. Then the noninteracting picture will prevail and no satellite peak would result. It is impossible to correlate this picture with an observation of fine splitting as was done for the subthreshold multiplets in La.

We also have performed a convolution based on the two-density-of-states model, Eq. (3), using the isochromat data of Chamberlain *et al.*[22] and the absorption coefficient data of Haensel *et al.*[38] The results are shown in Fig. 9. Above threshold, as for La, the agreement is not exact. Below threshold, the results do not resemble the multiplet structure observed and show, instead, something resembling a doublet.

TABLE I. Tentative interpretation of the fine-structure region in the $N_{4,5}$ SXAPS spectrum of Ce.

	SXA[a] peaks (eV)	$d\alpha/dE$[a] peaks (eV)	SXAPS peaks (eV)	ΔE[b] SXA	ΔE[b] $d\alpha/dE$
A[c]	101.25	101	103.2	1.95	2.2
B	103.48	103.1	105.0	1.52	1.9
C	104.56	104.5 (S)[d]	106.3 (S)	1.74	1.8
D	105.77	105.5	107.2	1.43	1.7
E	106.06				
F	106.58	106.3 (S)	108.2 (S)	1.62	1.9
G	108.06	107.8	110	1.94	2.2
H	108.93				
J	109.70				
K	110.36	109.8	112.6	2.24	2.8
L	111.52	111.2	113.7 (S)	2.18	2.5
			Total average ΔE[e]	1.8	2.1
			Partial average ΔE[e]	1.9	2.2

[a] Data from Ref. 31.

[b] ΔE is the energy difference between the SXA ($d\alpha/dE$) and the SXAPS peak positions.

[c] See Ref. 38 for letter designation and Ref. 39 for spectral term designation.

[d] S, shoulder.

[e] Total average ΔE is the average of all eight values. Partial average ΔE is the average of peak values only.

D. Ce $M_{4,5}$ region

In Fig. 10 we show the $M_{4,5}$ region of the Ce SXAPS. The top curve is for a fresh film at 3×10^{-10} Torr. The middle curve is from an early evaporation and shows a definite asymmetry in the negative peak, which may be attributed to the appearance of an additional shoulder in the total yield at slightly higher energy. In the lower curve of Fig. 10 we show the spectrum of a clean

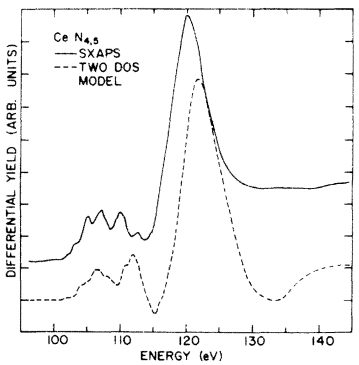

FIG. 9. Comparison of the Ce $N_{4,5}$ SXAPS spectrum (solid curve) with the two-density-of-states model calculation (dashed curve).

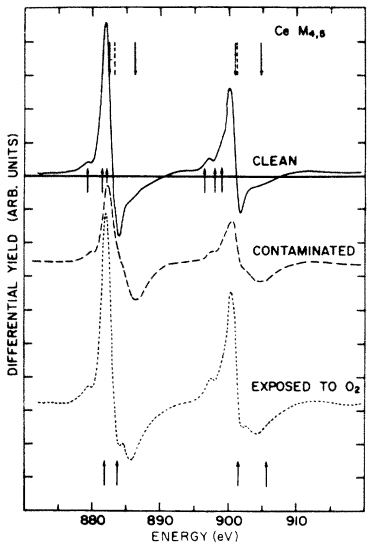

FIG. 10. SXAPS for the $M_{4,5}$ region of Ce. The dashed vertical lines mark the atomic core binding energies,[29] and the arrows pointing down mark the XPS peak positions.[32] The lower arrows show the peak positions for absorption measurements.[52] The noise is about the width of the line.

film exposed to oxygen at a pressure of 10^{-3} Torr for about 1 h. The spectrum is similar to that for clean Ce with the exception of the additional structure in the negative portion of both the M_5 and M_4 peaks. The first group of structures in each spectrum corresponds to the excitation of the $3d_{5/2}$ level, the second to the excitation of the $3d_{3/2}$ level, similar to La. The SXA spectrum of Ce differs markedly from that of its oxides[52] but multiplet structures are present in both. On the other hand, the emission spectra of Fisher and Baun[55] show only two lines, at 880.4 and 889.1 eV. Chamberlain *et al.*[22] studied the isochromat bremsstrahlung spectrum of Ce, sweeping across the $M_{4,5}$ region with the projectile electron energy. They found the same results as for La, i.e., a strong enhancement of the bremsstrahlung peak when the characteristic soft x-ray line begins to appear. Harte *et al.*[8] have calculated the SXAPS for Ce from the data of Chamberlain *et al.*,[22] obtaining good agreement with the experimental spectrum. We thus are facing the same resonance effect discussed for the $M_{4,5}$ spectrum of La. This gives a peak in the total yield (and thus a dispersionlike feature in the SXAPS) at 883.0 and 901.0 eV for the M_5 and M_4 regions, respectively. Due to the complexity of the expected multiplet structure, it is not possible to obtain the same neat picture as for La in associating SXAPS structures with SXA structures. Chamberlain *et al.*[22] found that the M_5 and M_4 lines started to appear at electron energies[58] of ~881 and ~897 eV, respectively. These two values are in fair agreement with the two threshold energies we observe at 877.5 and 895.5 eV.

Further discussion of the Ce $M_{4,5}$ region does not seem possible at this time. In La, the $M_{4,5}$ SXA and emission spectra were identical in shape, but for Ce there is a discrepancy, there being more, or less, lines in the absorption spectrum[52] than in the emission spectrum.[55] This is probably an artifact of the energy of the electron used to excite the emission spectrum, since there are bremsstrahlung resonances when it is near the $M_{4,5}$ resonance energy. Self-absorption effects may also play a role. As with the La $M_{4,5}$ region, the Ce $M_{4,5}$ SXAPS is not fit closely by α, $d\alpha/dE$, or the self-convolution model using α. The SXAPS and $d\alpha/dE$ spectra have an equal number of peaks, so, unlike La, the interacting projectile electron may not be bound in Ce when exciting the $M_{4,5}$ electrons. This suggestion was also made for the Ce $N_{4,5}$ excitations.

IV. EFFECTS OF Ce FILM CONTAMINATION

The atomic configuration for Ce is $(Xe)4f5d6s^2$. The ion in the metal is thought to contain one $4f$ electron. However, Ce also has a tetravalent state[59] in which the single f electron also is lost. Thus we have two oxides for Ce, Ce_2O_3, as for La, and CeO_2. This additional complexity for Ce has revealed itself in much of the experimental data. For example, only Ce of all the light rare earths, shows major changes in its absorption spectrum when exposed to air.[36,52] The studies of Fisher and Baun[55] revealed no such changes for Ce but they did occur for Yb, which also has two different valence states. Due to the vacuum conditions for many of these measurements it is quite possible that these changes reflect the difference between CeO_2 and Ce_2O_3 rather than between metal and oxide.

The SXAPS spectrum of Ce exposed to oxygen (Fig. 10) is similar to that for clean Ce with the exception of the additional structure in the negative portion of both the M_5 and M_4 peaks. The arrows at the bottom of the figure mark the peak positions in the absorption data of Bonnelle *et al.*[52] for Ce exposed to air. They attribute this rearrangement of peaks to the formation of CeO_2. Our oxide spectra do not show the additional peak which they observe at 905.6 eV and, furthermore, the weak structures below each main peak still resemble the clean Ce spectrum. We conclude that the additional two small peaks may instead signal the formation of Ce_2O_3 on the surface. Such an interpretation seems somewhat speculative but there is evidence that the oxidation process for Ce may depend on the

oxygen exposures involved.[60]

We use the $N_{4,5}$ region as a guide. After the heavy exposure to oxygen, the $N_{4,5}$ region (Fig. 7) still showed the five peaks below threshold which are indicative of the tripositive Ce ion. We conclude that the exposure to O_2 led to the formation of Ce_2O_3 which, if quite protective and thin, may have allowed the incident electron to probe both oxide and clean metal. This would imply that the protective layer is at most a few monolayers thick. Another possible explanation is that we have a very small concentration of CeO_2 in a matrix of Ce_2O_3. The CeO_2 ions have the slightly larger binding energy due to reduced outer shielding. The situation here is not well understood, however, since Suzuki *et al.*[61] suggest that Ce_2O_3 resulted when Ce was exposed to air. Their XPS spectra in the region of $4d$ excitations had similar features for this oxide and for CeF_3 which differed from their CeO_2 spectra. This suggests, in agreement with our data, that Ce_2O_3 is the more stable phase for large exposures. Note that another oxide of Ce, CeO, has been detected.[62]

An appendix discusses spectra of Ce that appear to arise from Ce^{4+} ions in Ce metal rather than CeO_2.

V. SUMMARY

The SXAPS spectra of the $3d$ and $4d$ states in La and Ce do not fit one-electron models and give little information about the density of empty states above the Fermi Level. The $M_{4,5}$ and $N_{4,5}$ SXAPS can be explained qualitatively with the two-density-of-states model of Wendin, along with x-ray absorption data, except for the extra splitting in the $N_{4,5}$ spectrum of La and a shape discrepancy in the $N_{4,5}$ spectrum of Ce. The former can be explained qualitatively by allowing the projectile electron to be localized on the excited ion.

Effects of contamination have been observed, but a simultaneous study of what the contaminants are is needed. The correlation of SXAPS with SXA and x-ray emission data has been pointed out, but some problems remain. Little of the x-ray work was done in the requisite ultrahigh vacuum and there are some discrepancies in the spectra recorded by different investigators.[63] Soft x-ray absorption and emission spectra on very clean metal, as well as on an oxide or fluoride, should be repeated, with auxiliary measurements made to monitor sample decomposition from the electron beam. A number of the incomplete explanations we have given involve discrepancies in other spectra, and unknown calculated quantities, usually involving binding energies.

We recently became aware of the SXAPS work of Chamberlain and Baun[64] on Ce. Our results are in good agreement with their reported spectra, apart from some minor line-shape discrepancies in the $N_{4,5}$ spectra. Our Ce $M_{4,5}$ spectra closely resemble their results for short "beam-on" times and suggest that their observed line-shape changes, which were attributed to beam-induced annealing, may be due to other time-dependent effects. Also, our interpretation suggests that the extra electron may not be bound on the excited Ce ion, contrary to the interpretation of Chamberlain and Baun.

Kanski *et al.*[65] have recently studied the M_5 excitation spectra by SXAPS, x-ray excited electron APS, and x-ray photoelectron spectroscopy. Their SXAPS spectrum are similar to ours except that the shoulder at 834 eV is better resolved in their spectrum. They discuss the role of the rest of the system on the excitation energy to $4f$ states in La, showing that all spectroscopies "overestimate" the position of these states above E_F, but by varying amounts.

APPENDIX: Ce (IV)

As mentioned earlier, the $4f$ orbital of Ce is just sufficiently bound to make the Ce ion trivalent. Vickery[66] points out that of all the lanthanides, Ce is the only one which can give rise to a stable 4+ ion. He suggests that it is no more difficult to remove the $4f$ electron than it is to remove the $5d$ or $6s$ electrons. During our study of Ce it became evident that for a short time, at least, the surface of our film consisted of Ce^{4+} ions. The conditions which prompted this valency change are not clear. Three evaporations had been made and the $N_{4,5}$ spectra recorded after each consistently showed the five peaks below threshold as discussed above. The fourth evaporation yielded spectra like the dashed curve shown in Fig. 11. The pressure during evaporation did not rise above 9×10^{-9} Torr, and dropped immediately thereafter to 1.5×10^{-10} Torr. This process was repeated three more times and each film showed this same spectrum. The main peak is not shifted, but the high-energy side seems broader, with a weak feature around 130 eV. Moreover, the structure below threshold now appears as a doublet, with some weaker shoulders. The threshold is still in agreement with the earlier Ce data.

A scan of the $M_{4,5}$ region after the seventh evaporation resulted in the bottom curve of Fig. 12. The $M_{4,5}$ peaks show new splitting of unequal intensity. At this time the higher-energy peak at 883.7 eV was the stronger of the two M_5 features. This film was held at a base pressure of 1×10^{-10} Torr for several hours. The system was then turned on again and both the $N_{4,5}$ and $M_{4,5}$ regions still

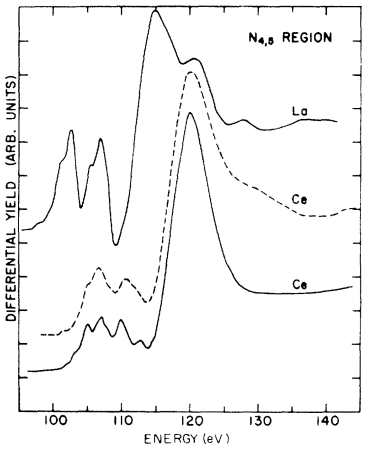

FIG. 11. $N_{4,5}$ SXAPS for tetravalent Ce (dashed curve). The solid curves show the $N_{4,5}$ spectra for La and trivalent Ce metal.

showed the new structure. A series of evaporations was then made as indicated by the curves of Fig. 12 and the intensities of the new second peaks gradually reduced, reverting to the original $M_{4,5}$ spectrum shown earlier. At the same time the $N_{4,5}$ spectrum returned to its original form, with five peaks below threshold. This sequence was originally thought to represent a mixture of Ce_2O_3 and Ce metal. The fairly close resemblance of the $N_{4,5}$ spectra of La and this series of Ce runs (Fig. 11) leads us to conclude that the Ce film during these runs consisted of Ce^{4+} ions, i.e., an ion like La^{3+} but with an extra nuclear charge. The entire sequence of Fig. 12 covers a period of about 10 h. Each individual spectrum was reproducible and only a new evaporation caused the intensity changes. We emphasize that at all times other than during evaporation, our working pressure was below 5×10^{-10} Torr. We conclude then that the films represent metallic Ce rather than oxide. This idea is supported by the $N_{4,5}$ region (Fig. 11) which shows a broad main peak without the high-energy minimum which is characteristic of the contaminated films (Fig. 7). We observed this same transformation of the Ce $N_{4,5}$ fine structure in an earlier study using a different piece of Ce, but cut from the same batch as the present evaporant.

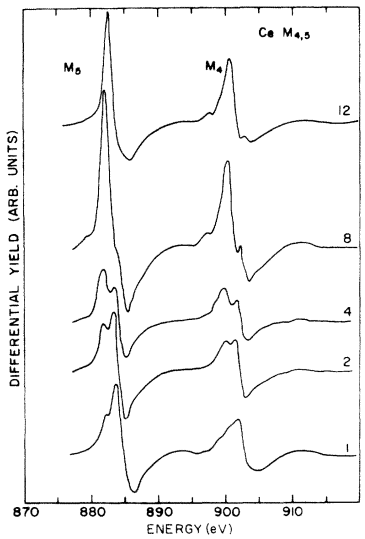

FIG. 12. Series of spectra obtained for the Ce $M_{4,5}$ region during the transition from tetravalent to trivalent Ce. The numbers on the right indicate the film from which each spectrum was obtained, relative to the third evaporation (bottom curve).

The SXA data of Haensel *et al.*[38] lend further support to the La-like configuration for Ce. Their results for Ce oxide show two peaks, at 103.45 and 108.21 eV, with some weaker structure. We assume that this represents CeO_2. Their data give peaks for $d\alpha/dE$ at 103.2 and 107.9 eV. The low-energy SXAPS peaks are at 105.2, 106.7, 110.6, and 111.8 eV. The separations ΔE of the SXAPS peaks from the $d\alpha/dE$ peaks are 2.4 and 3.7 eV. This same quantity for La^{3+} was 4.4 and 5.8 eV, respectively. The empty $4f$ states in Ce^{4+} appear to be slightly further above the ionization threshold than are the $4f$ states in Ce^{3+}, which is what we expect. Also, the $4f$ states in Ce^{4+} are pulled down towards the threshold level relative to those of La^{3+}, as expected, due to the extra nuclear charge in Ce^{4+}.

The splitting of the $M_{4,5}$ peaks in Fig. 12 is 1.6 eV. For the CeO_2 data of Bonnelle *et al.*,[52] the shift upon oxidation is about 1.8 eV for the main M_5 peak and 2.4 eV for the M_4 peak, slightly greater than our splitting of 1.6 eV for the M_4 and M_5 doublets. (Note in Fig. 10, we see no shift upon exposing Ce to O_2.)

The data presented here strongly suggest that we had for some time Ce^{4+} ions in a metallic state. We cannot state with confidence the reason for this valency change nor can we rule out the existence of CeO_2. One possible explanation is that the $4f$ orbital is emptied due to the elevated sample temperature. Habermann and Daane[67] have suggested this depopulation as a possible cause for the unusually high heat of sublimation for Ce. The argument is that above room temperature, the $4f$ electron is thermally excited into the conduction band. If a d-symmetry orbital is occupied, the cohesive energy would be increased relative to that of La as is experimentally observed. We do not know the substrate temperature in our experiment, but it is certainly well above room temperature due to the

nearby tungsten filament and to electron beam heating. However, these conditions were not altered much during the Ce runs and another explanation is probably needed. It may be a specific surface effect. Ce should be further studied using a heated substrate in conjunction with Auger analysis to determine whether the surface represents metallic Ce^{4+} or CeO_2.

---

*Work performed for the U. S. Energy Research and Development Administration under Contract No. W-7405-eng-82.

†Present address: Dept. of Physics, Montana State University, Bozemen, Mont. 59715.

‡On leave from Gruppo Nazionale di Struttura della Materia del C.N.R., Sezione di Roma, Istituto di Fisica dell' Universitá, Rome, Italy (present address).

§Present address: Academic Computing Services, University of Northern Iowa, Cedar Falls, Ia. 50613.

[1]B. Dev and H. Brinkman, Ned. Tijdschr. Vacuumtechn. 8, 176 (1970).

[2]J. E. Houston and R. L. Park, J. Chem. Phys. 55, 4601 (1971).

[3]R. L. Park and J. E. Houston, Phys. Rev. B 6, 1073 (1972).

[4]P. O. Nilsson and J. Kanski, Phys. Lett. A 41, 217 (1972).

[5]P. O. Nilsson and J. Kanski, Surf. Sci. 37, 700 (1973).

[6]J. Kanski and P. O. Nilsson, Phys. Lett. A 45, 399 (1973).

[7]M. B. Chamberlain and W. L. Baun, J. Vac. Sci. Technol. 11, 441 (1974).

[8]W. E. Harte, P. S. Szczepanek, and A. J. Leyendecker, Phys. Rev. Lett. 33, 86 (1974).

[9]M. S. Murthy and P. A. Redhead, J. Vac. Sci. Technol. 11, 837 (1974).

[10]K. N. Ramachandran and C. D. Cox, J. Vac. Sci. Technol. 11, 579 (1974).

[11]P. S. Szczepanek and W. E. Harte, Phys. Lett. A 49, 377 (1974).

[12]P. O. Nilsson, J. Kanski, and G. Wendin, Solid State Commun. 15, 287 (1974).

[13]J. E. Houston and R. L. Park, J. Vac. Sci. Technol. 8, 91 (1971).

[14]J. E. Houston and R. L. Park, Solid State Commun. 10, 91 (1972).

[15]J. C. Tracy, Appl. Phys. Lett. 19, 353 (1971).

[16]J. C. Tracy, J. Appl. Phys. 43, 4164 (1972).

[17]R. L. Park and J. E. Houston, J. Vac. Sci. Technol. 11, 1 (1974).

[18]G. Wendin, *Proceedings of the International Conference on Vacuum-Ultraviolet Radiation Physics, Hamburg, 1974* (Vieweg-Pergamon, Braunschweig, 1974), p. 252.

[19]B. Coqblin, J. Phys. (Paris) Suppl. 32, Ci-599 (1971).

[20]J. Appel, Phys. Rev. B 8, 1079 (1973).

[21]R. J. Liefeld, A. F. Burr, and M. B. Chamberlain, Phys. Rev. A 9, 316 (1974).

[22]M. B. Chamberlain, A. F. Burr, and R. J. Liefeld, Phys. Rev. A 9, 663 (1974).

[23]J. Kanski, Ph.D. thesis (Chalmers University of Technology, Goteborg, Sweden, 1974) (unpublished).

[24]J. E. Houston and R. L. Park, Rev. Sci, Instrum. 43, 1437 (1972).

[25]W. L. Baun, M. B. Chamberlain, and J. S. Soloman, Rev. Sci. Instrum. 44, 1419 (1973).

[26]R. J. Smith, Ph.D. thesis (Iowa State University, 1975) (unpublished).

[27]R. G. Musket and S. W. Taatjes, J. Vac. Sci. Technol. 9, 1041 (1972).

[28]C. Webb and P. M. Williams, Phys. Rev. Lett. 33, 824 (1974).

[29]J. A. Bearden and A. F. Burr, Rev. Mod. Phys. 39, 125 (1967).

[30]Electron excitation and photoabsorption have different selection rules, determined by the transition matrix element. Even though the matrix elements have been neglected, the substitution $\alpha(E) \approx N(E - E_c)$ leading to Eq. (2) might seem rather arbitrary. However, we feel justified in doing so by the fact that far above the excitation energy, the inelastic cross sections follow closely the optical selection rules. For this reason, electron energy loss spectra, in the limit of small transferred momenta, are very similar to the optical spectra. In order to check the validity of these assumptions near threshold, we calculated with Eq. (2) the expected SXAPS for the $L_{2,3}$ region of Cr. The result, obtained using SXA data of Fisher,[49] agrees very well with the experimental SXAPS of Park and Huston.[48]

[31]P. Rabe, Ph.D. thesis (Universität Hamburg, 1974) (unpublished).

[32]I. Nagakura, T. Ishii, and T. Sagawa, J. Phys. Soc. Jpn. 33, 754 (1972).

[33]R. Smith, M. Piacentini, and D. W. Lynch, Phys. Rev. Lett. 34, 476 (1975).

[34]S. Suzuki, I. Nagakaura, T. Ishii, T. Satoh, and T. Sagawa, Phys. Lett. A 41, 95 (1972).

[35]V. A. Fomichev, T. M. Zimkina, S. A. Gribovskii, and I. Zhukova, Fiz. Tverd. Tela 9, 1490 (1967) [Sov. Phys.-Solid State 9, 1163 (1967)].

[36]T. M. Zimkina, V. A. Fomichev, S. A. Gribovskii, and I. I. Zhukova, Fiz. Tverd. Tela 9, 1447 (1967) [Sov. Phys.-Solid State 9, 1128 (1967)].

[37]I. Nagakura, O. Aita, K. Ichikawa, S. Suzuki, S. Kono, T. Ishiii, and T. Sagawa, Third International Conference on Vacuum-Ultraviolet Radiation Physics, Tokyo, 1971 (unpublished).

[38]R. Haensel. P. Rabe, and B. Sonntag, Solid State Commun. 8, 1845 (1970).

[39]J. Sugar, Phys. Rev. B 5, 1785 (1972).

[40]A. F. Starace, Phys. Rev. B 5, 1773 (1972).

[41]J. L. Dehmer and A. F. Starace, Phys. Rev. B 5, 1792 (1972).

[42]J. L. Dehmer, A. F. Starace, U. Fano, J. Sugar, and J. W. Cooper, Phys. Rev. Lett. 26, 1521 (1971).

[43]F. Herman and S. Skillman, *Atomic Structure Calculations* (Prentice-Hall, Englewood Cliffs, N.J., 1963).

[44]A. F. Starace, J. Phys. B 7, 14 (1974).

[45]D. W. Lynch and C. G. Olson, *Proceedings of the International Conference on Vacuum-Ultraviolet Radiation Physics, Hamburg, 1974* (Vieweg-Pergamon, Braunschweig, 1974), p. 258.

[46]J. Daniels, C. V. Festenburg, H. Raether, and K. Zeppenfeld, Springer Tracts Mod. Phys. 54, 77 (1970).
[47]P. Trebbia and C. Colliex, Phys. Status Solidi B 58, 523 (1973).
[48]J. E. Houston and R. L. Park, in *Electron Spectroscopy*, edited by D. A. Shirley (North-Holland, Amsterdam, 1972) p. 895.
[49]D. W. Fischer, Phys. Rev. B 4, 1778 (1971).
[50]U. Fano and J. W. Cooper, Rev. Mod. Phys. 40, 441 (1968).
[51]We almost reproduced the observed high-energy line shape in Fig. 5(a) by summing two Gaussians of 1-eV width, with peak energies separated by 1.75 eV. Varying the intensity A of the high-energy Gaussian with respect to the intensity ($A=1$) of the other, we found best agreement with curve (a) for $A=0.1$. For $A=0.2$ a pronounced shoulder appears, as in Fig. 5(c), and for $A=0.5$ two negative peaks of the same intensity are well resolved, as in Murthy and Redhead's data.[9] Note that the zero crossing of the leading structure shifts to higher energies as the amount of "contamination" increases.
[52]C. Bonnelle, R. C. Karnatak, and J. Sugar, Phys. Rev. A 9, 1920 (1974).
[53]J. Sugar, Phys. Rev. A 6, 1764 (1972).
[54]J. M. Mariot and R. C. Karnatak, J. Phys. F 4, 1223 (1974).
[55]D. W. Fischer and W. L. Baun, in *Advances in X-Ray Analysis*, edited by J. B. Newkirk, G. R. Maller, and H. G. Pfeiffer (Plenum, New York, 1968), Vol. 11, p. 230.
[56]At $E_A \approx E_m$ a second low-energy structure has developed, peaking ~3 eV below the M_5 line. This satellite line is present for $E_0 > E_m$, which is the condition for soft x-ray emission measurements.[54,55] The satellite appears in the M_4 region, too, and in the Ce spectra. Since it does not seem to be a major feature, we shall neglect it in the discussion. If it is a static feature, it will not contribute additional structure in SXAPS, which measures a derivative.
[57]S. Geltman, *Topics in Atomic Collision Theory* (Academic, New York, 1969), p. 160.
[58]We have used the electron energies as published in Ref. 21 for La, but for Ce, the authors of Ref. 22 did not correct for the work function of their Th-Ir cathode. We have thus added 2.7 eV to the electron energies we quote from Ref. 22.
[59]D. Brown, *Halides of the Lanthanides and Actinides* (Wiley, London, 1968), p. 3.
[60]C. R. Helms and W. E. Spicer, Appl. Phys. Lett. 21, 237 (1972).
[61]S. Suzuki, T. Ishii, and T. Sagawa, J. Phys. Soc. Jpn. 37, 1334 (1974).
[62]K. A. Gschneidner and J. T. Waber, J. Less-Common Met. 6, 354 (1964).
[63]See for example D. Ottewell, E. A. Stewardson, and J. E. Wilson, J. Phys. B 6, 2184 (1973) for the $M_{4,5}$ x-ray absorption of Ce, CeO_2, Ce oxide and CeF_3, and compare to the data of Ref. 52.
[64]M. Chamberlain and W. L. Baun, J. Vac. Sci. Technol. 12, 1047 (1975).
[65]J. Kanski, P. O. Nilsson, and I. Curelaru, J. Phys. F 6, 1073 (1976).
[66]R. C. Vickery, *Chemistry of the Lanthanons* (Butterworths, London, 1953), p. 60.
[67]C. E. Haberman and A. H. Daane, J. Chem. Phys. 41, 2818 (1964).